American Journal of Fluid Dynamics 2014, 4(2): 69-78
DOI: 10.5923/j.ajfd.20140402.03

LES Modelling of Nitric Oxide (*NO*) Formation in a Propane-Air Turbulent Reacting Flame

Sreebash C. Paul[1], Manosh C. Paul[2], Suvash C. Saha[3,*]

[1]Department of Arts and Sciences, Ahsanullah University of Science and Technology, Dhaka 1208, Bangladesh
[2]Systems, Power & Energy Research Division, School of Engineering, University of Glasgow, Glasgow G12 8QQ, UK
[3]School of Chemistry, Physics and Mechanical Engineering, Queensland University of Technology, 2 George St., GPO Box 2434, Brisbane QLD 4001, Australia

Abstract Large Eddy Simulation (LES) technique is applied to investigate the nitric oxide (*NO*) formation in the propane-air flame inside a cylindrical combustor. In LES a spatial filtering is applied to the governing equations to separate the flow field into large scale eddies and small scale eddies. The large scale eddies which carry most of the turbulent energy are resolved explicitly while the unresolved small scale eddies are modelled. A Smagorinsky model with model constant C_s = 0.1 as well as a dynamic model has been employed for modelling of the sub-grid scale eddies, while the nonpremixed combustion process is modelled through the conserved scalar approach with laminar flamelet model. In *NO* formation model, the extended Zeldovich (thermal) reaction mechanism is taken into account through a transport equation for *NO* mass fraction. The computational results are compared with those of the experimental results investigated by Nishida and Mukohara [1] in co-flowing turbulent flame.

Keywords Large Eddy Simulation, Turbulent Flow, Combustion, Laminar Flamelet, *NO* formation, Sub-Grid Scale

1. Introduction

In every circumstances where combustion occurs, the formation of Nitrogen Oxides (NO_x) are unavoidable. From a home open fire to a coal fired power plant, NO_x is formed as an undesired product and a contributor to air pollution and health problems. Due to the increasing concerns over the environmental pollution, the understanding of the NO_x formation mechanism during the combustion process and of the development of their reduction technologies is essential for the efficient design of combustion devices. But, one of the great challenges in predicting the formation of the NO_x in a combustion process is the chemical time-scale, which is slow.

NO_x is used to refer to the nitric oxide *NO* and the nitrogen oxide NO_2. Typically 95% of the total NO_x emissions is nitric oxide, *NO*, which is the primary form in combustion products. The nitric oxide *NO* is subsequently oxidized to NO_2 in the atmosphere.

There are four different routes or mechanisms in the formation of NO_x, which were identified by Bowman [2]. These are the thermal *NO* route, the prompt *NO* route, the N_2O (nitrous oxide) route, and the fuel-bound nitrogen route.

But, it is known that in nonpremixed combustion of hydrocarbon fuels, the first two mechanisms dominate the process of nitric oxide, *NO*, formation. The thermal *NO* also well-known as the Zeldovich *NO* proposed by Zeldovich [3], which dominantly depends on its local temperature and reactants (O_2 and N_2). The prompt or Fenimore *NO* mechanism proposed by Fenimore [4], is formed through hydro-carbon radical reaction with molecular nitrogen under fuel-rich condition. In most flames, especially those from nitrogen-containing fuels, the prompt mechanism is responsible for only a small fraction of the total NO_x.

Meunier *et al.* [5] investigated the NO_x emissions from turbulent propane diffusion flames experimentally as well as numerically. In numerical investigation both the thermal and prompt *NO* reaction mechanism were used to predict *NO* formation. The equations were closed by k-ϵ turbulence model where as the combustion was modelled using the stretched laminar flamelet model and the probability density function (PDF) method.

Formation characteristics of the nitric oxide in a three-stage air/LPG flame has been investigated both experimentally and numerically by Kim *et al.* [6] including both the thermal and the prompt *NO* formation mechanism through a conservation equation of *NO* mass fraction. The computed results were compared with the experimental measurements.

* Corresponding author:
s_c_saha@yahoo.com (Suvash C. Saha)
Published online at http://journal.sapub.org/ajfd

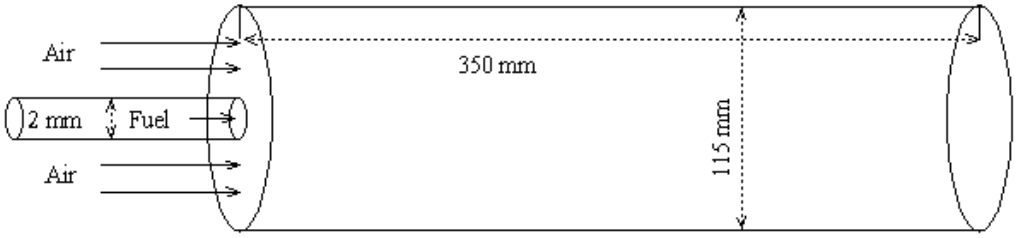

Figure 1. A schematic of the cylindrical combustor with short computational domain

For the hydrogen jet diffusion flame, a prediction method for *NO* applicable to LES was presented by Taniguchi *et al.* [7]. To model *NO* production, they considered the extended Zeldovich mechanism with the quasi-steady state approximation of the nitric atom through the balance equation of *NO* mass fraction. In LES, they neglected the SGS contribution to the *NO* production.

Modeling of radiation and *NO* formation in turbulent nonpremixed flames using a flamelet/progress variable formulation has been investigated by Ihme and Pitsch [8]. In *NO* production model, a transport equation for the *NO* mass fraction was considered, and they obtained the chemical source term from the flamelet library. The *NO* model formulation was analyzed separately for the thermal, nitrous oxide, and prompt *NO* reaction mechanisms.

Chun *et al*. [9] performed a numerical study on extinction and NO_x formation in nonpremixed flames with syngas fuel. Numerical simulations were done in a quasi-one dimensional counterflow configuration using the OPPDIF code adopting GRI-Mech 3.0 for the chemical reaction mechanism. They have considered a reaction path diagram to analyze NO_x formation pathways along with the thermal NO_x formation mechanism. They found that the *NO* production through the thermal mechanism was weakened more than that through the non-thermal mechanism, and most of the NO_x production started from the $N_2 \rightarrow NNH$ pathway.

In this paper LES technique has been applied to investigate the *NO* formation in the non-premixed propane-air turbulent combustion process within a cylindrical combustor. A schematic of computational domain is shown in Fig. 1. Gaseous propane (C_3H_8) is injected through a circular nozzle of an internal diameter of $2mm$ at the centre of the combustor inlet while the preheated air of temperature $773K$ with an averaged velocity of $0.96ms^{-1}$ is supplied through the circular inlet of $115mm$ internal diameter into the $350mm$ long combustion chamber. The overall equivalence ratio is 0.6 so that burning occurs in a fuel-rich nonpremixed combustion mode, which produces various forms of hydrocarbons in the combustion products. The average fuel velocity measured by [1] at the inlet is $30ms^{-1}$. A Smagorinsky model with $C_s = 0.1$ as well as its dynamic calibration has been employed to model the sub-grid scale stresses, while the non-premixed combustion process is modelled through the conserved scalar approach with laminar flamelet model. The *NO* production mechanism is modelled through a balance equation for *NO* mass fraction. The extended Zeldovich (thermal) reaction mechanism is taken into account to model the *NO* production.

This paper is structured in the following order. The modelling of the *NO* formation is presented in §2, followed by the Mathematical formulation for LES including the sgs modelling and the conserved scalar approach to combustion modelling in §3. In §4 the numerical procedure and the necessary boundary conditions used in the LES are described. Results and discussion are presented in §5. In §6 a general conclusion of this paper is made.

2. Nitric Oxide (*NO*) Prediction Model

In a non-premixed combustion process a high temperature is occurred at the stoichiometric interface where the thermal reaction mechanism of *NO* dominates its formation. So, the maximum flame temperature is the most important parameter that determines the potential for *NO* formation. The high *NO* levels that occur in practical systems can only be reduced by reducing the thermal *NO* formation. In the present *NO* formation model, the extended Zeldovich (thermal) reaction mechanism proposed by Zeldovich [3], is taken into account through the solution of a transport equation for *NO* mass fraction (see equation (8)). The extended Zeldovich reaction mechanism has the following three reactions;

$$N_2 + O \xrightarrow{K_1} NO + N \tag{1}$$

$$O_2 + N \xrightarrow{K_2} NO + O \tag{2}$$

$$OH + N \xrightarrow{K_3} NO + H \tag{3}$$

According to the above reactions, the formation rate of *NO* is

$$\frac{d[NO]}{dt} = k_1[N_2][O] + k_2[O_2][N] + k_3[OH][N] \tag{4}$$

and the rate for nitrogen atoms is

$$\frac{d[N]}{dt} = k_1[N_2][O] - k_2[O_2][N] - k_3[OH][N] \tag{5}$$

Assuming a quasi steady state assumption of the nitrogen atoms, i.e., $d[N]/dt \approx 0$, , yields the rate of formation of *NO* as

$$r_{NO} = \frac{d[NO]}{dt} = 2k_1[N_2][O] \tag{6}$$

where $[N2] = \rho Y_{N2}/M_{N2}$, $[O] = \rho Y_O/M_O$; $M_{N2} = 28\ kg/kmol$ and

$M_O = 16\ kg/kmol$ are the molar mass of N_2 and O respectively. The reaction rate, k_1, based on Baulch *et al.* [10, 11] is taken as

$$k_1 = 4.1\times10^{10}\exp\left(-\frac{318}{RT}\right) \tag{7}$$

where $R = 8.314472 J.K-1.mol-1$ is the universal gas constant.

The transport equation for *NO* is written as

$$\frac{\partial(\rho Y_{NO})}{\partial t}+\frac{\partial\left(\rho u_j Y_{NO}\right)}{\partial x_j}=\frac{\partial}{\partial x_j}\left(\Gamma\frac{\partial Y_{NO}}{\partial x_j}\right)+\rho S(Y_{NO}) \tag{8}$$

where Y_{NO} is the mass fraction of *NO*.

The source term, $\rho S(Y_{NO})$, for the formation of *NO* mass fraction per unit volume is therefore expressed as

$$\rho S\left(Y_{NO}\right)=M_{NO}r_{MO} \tag{9}$$

where M_{NO} is the molecular weight of *NO*.

3. Mathematical Formulation for LES

In LES, a spatial filtering operation is applied to the governing equations of motions to separate the large scale (resolved scale) flow field from the small scale (sub-grid scale), Leonard [12]. Employing the density weighted Favre-filtered function, Favre [13] to the continuity equation, Navier- Stokes equations, the mixture fraction (conserved scalar) equation, and the conservation equation for *NO* mass fraction equation gives:

$$\frac{\partial\overline{\rho}}{\partial t}+\frac{\partial\left(\overline{\rho\widetilde{u}}_j\right)}{\partial x_j}=0 \tag{10}$$

$$\frac{\partial\left(\overline{\rho}\tilde{u}_i\right)}{\partial t}+\frac{\partial\left(\overline{\rho}\tilde{u}_i\tilde{u}_j\right)}{\partial x_j} =-\frac{\partial\overline{p}}{\partial x_i}+\frac{\partial}{\partial x_j}\left[2\mu\overline{S}_{ij}-\frac{2}{3}\mu\overline{S}_{kk}\delta_{ij}\right]-\frac{\partial\tau_{ij}}{\partial x_j} \tag{11}$$

$$\frac{\partial\left(\overline{\rho}\widetilde{\xi}\right)}{\partial t}+\frac{\partial\left(\overline{\rho\widetilde{u}}_j\widetilde{\xi}\right)}{\partial x_j}=\frac{\partial}{\partial x_j}\left(\Gamma\frac{\partial\widetilde{\xi}}{\partial x_j}\right)-\frac{\partial J_j^{sgs}}{\partial x_j} \tag{12}$$

$$\frac{\partial\left(\overline{\rho}\tilde{Y}_{NO}\right)}{\partial t}+\frac{\partial\left(\overline{\rho}\tilde{u}_j\tilde{Y}_{NO}\right)}{\partial x_j} =\frac{\partial}{\partial x_j}\left(\Gamma\frac{\partial\tilde{Y}_{NO}}{\partial x_j}\right)+\rho\tilde{S}\left(\tilde{Y}_{NO}\right)-\frac{\partial\Phi_j^{sgs}}{\partial x_j} \tag{13}$$

where t is time; x_j is any of the three coordinate directions; u_j is any of the three velocity components; p is the pressure; ρ is the density, which, in reacting flows, varies due to the heat release from the chemical reaction and on the chemical composition of the fluid. μ is the molecular viscosity, $S_{ij}=\frac{1}{2}\left(\frac{\partial u_i}{\partial x_j}+\frac{\partial u_j}{\partial x_i}\right)$ is the strain rate, δ_{ij} is the kronecker delta, ξ is the conserved scalar or mixture fraction and $\Gamma=\frac{\mu}{Pr}=\frac{\mu}{Sc}$ is the diffusion coefficient.

The instantaneous source term, $\rho\widetilde{S}\left(\widetilde{Y}_{NO}\right)$, in conservation equation (13) for *NO* mass fraction is written as,

$$\rho\widetilde{S}\left(\widetilde{Y}_{NO}\right)=M_{NO}\widetilde{r}_{NO} \tag{14}$$

The *NO* production rate, r_{NO}, is a function of the flame temperature and the concentrations of N_2 and O (see equations (6) and (7)), which in turn can be expressed as a function of mixture fraction through the flamelet (Fig. 2) generated at a strain rate of $15s^{-1}$. A details of reaction mechanism and the flamelet calculations can be found in Leung [14]. The flamelet temperature is adjusted to account for the radiative heat loss to the combustor walls by using the following relation, Fairweather *et al*. [15]:

$$T(\xi)=T_{ad}(\xi)\left[1-\chi\left(\frac{T_{ad}(\xi)}{T_{ad,\max}}\right)^4\right] \tag{15}$$

where the radiative fraction, χ, is taken as 0.2, and T_{ad} represents the adiabatic flamelet temperature.

The variation of the instantaneous *NO* production rate with the variation of the mixture fraction variance, ξ'^2, is presented in Fig. 3. This figure shows that the peak value of the the *NO* production rate decreases in magnitude and also shifts to larger values of the mixture fraction with the increasing values of ξ'^2. The Favre-averaged *NO* production rate, $\widetilde{r}_{NO}$, for *NO* formation may therefore be determined by

$$\widetilde{r}_{NO}\left(\widetilde{\xi}\right)=\int_0^1 r_{NO}\widetilde{P}(\xi)d\xi\widetilde{\xi}'^2 \tag{16}$$

where $\widetilde{P}(\xi)$ is the β-pdf (probability density function) constructed from predicted values of the conserved scalar, $\widetilde{\xi}$, and the sub-grid scalar variance, $\widetilde{\xi}'^2$. Due to high peak appeared in *NO* production rate, it is convenient to use a piece-wise polynomial fitting approach (for details see, Paul [16]) for the best data fitting of the r_{NO}. Thus, a piece-wise polynomial fitting approach is used to integrate the β-pdf.

The most famous and still widely used model for the subgrid scale stress is that of the Smagorinsky model [17]. The model is based on an eddy viscosity assumption and of the form of

$$\tau_{ij}-\frac{1}{3}\delta_{ij}\tau_{kk}=-2\overline{\rho}\left(C_s\Delta\right)^2\left|\overline{S}\right|\overline{S}_{ij} \tag{17}$$

where Δ is the filter width and $\left|\overline{S}\right|=\sqrt{2\overline{S}_{ij}\overline{S}_{ij}}$ is the

magnitude of the large scale strain rate tensor, $\overline{S}_{ij}$. Two computations have been performed, one with $C_s = 0.1$ (Case1) and another one with its dynamically calibrated values (Case2), proposed by Germano *et al*. [18].

For the subgrid scale scalar fluxes, J_j^{sgs}, a gradient model, proposed by Schmidt and Schumann [19], of the form

$$J_j^{sgs} = -\overline{\rho}\Gamma_{sgs}\frac{\partial\widetilde{\xi}}{\partial x_j} = -\frac{\overline{\rho}\upsilon_{sgs}}{\sigma_{sgs}}\frac{\partial\widetilde{\xi}}{\partial x_j} \qquad (18)$$

is applied, where σ_{sgs} is a constant sub-grid scale Prandtl/Schmidt number which is assigned a value of 0.7.

In the *NO* model, we have used the same gradient model of Schmidt and Schumann [19] for modelling the subgrid scale *NO* mass fraction fluxes, Φ_j^{sgs}.

The conserved scalar modelling approach with the laminar flamelet model, Peters [20], is applied to model the combustion. In this approach, it is assumed that the chemical reaction rates are fast compared to the rate at which the reactants mix. The mixing process is described by a conserved scalar which is also known as the mixture fraction. It is then considered that the instantaneous species concentrations are a unique function of this mixture fraction. Since this functional dependence is highly nonlinear, the mean or filtered values are obtained via the probability density function of the mixture fraction, Bilger [21]. The filtered density ($\overline{\rho}$) and density weighted thermochemical variables ($\widetilde{\phi}$) are obtained by integrating over a β - probability density function, once the density weighted mixture fraction, $\widetilde{\xi}$, and its sub-grid scale variance are known. Further details of this model are found in Paul [16], Paul *et al*. [22] and di Mare *et al*. [23].

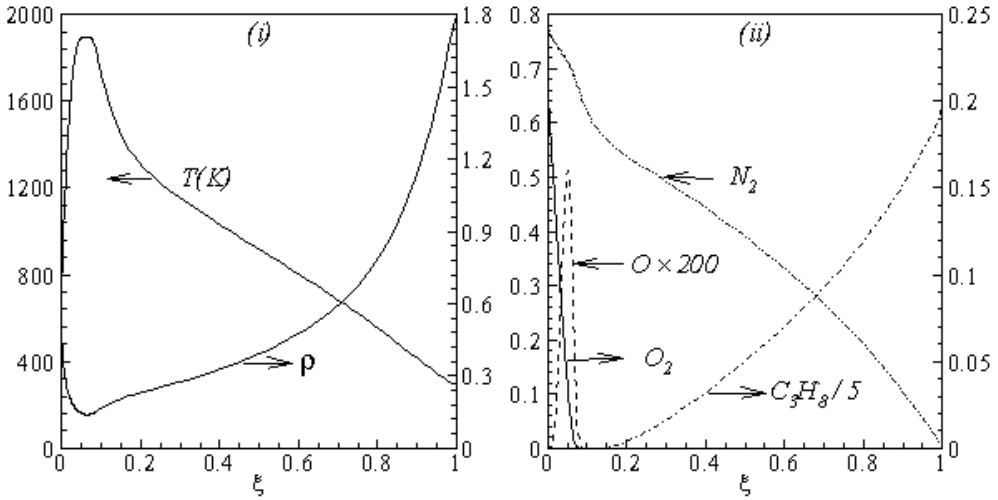

Figure 2. Laminar flamelet calculation for strain rate of $15s^{-1}$: dependance of (i) temparature and density; and (ii) mole fractions of C_3H_8, N_2, O and O_2, on the mixture fraction, ξ

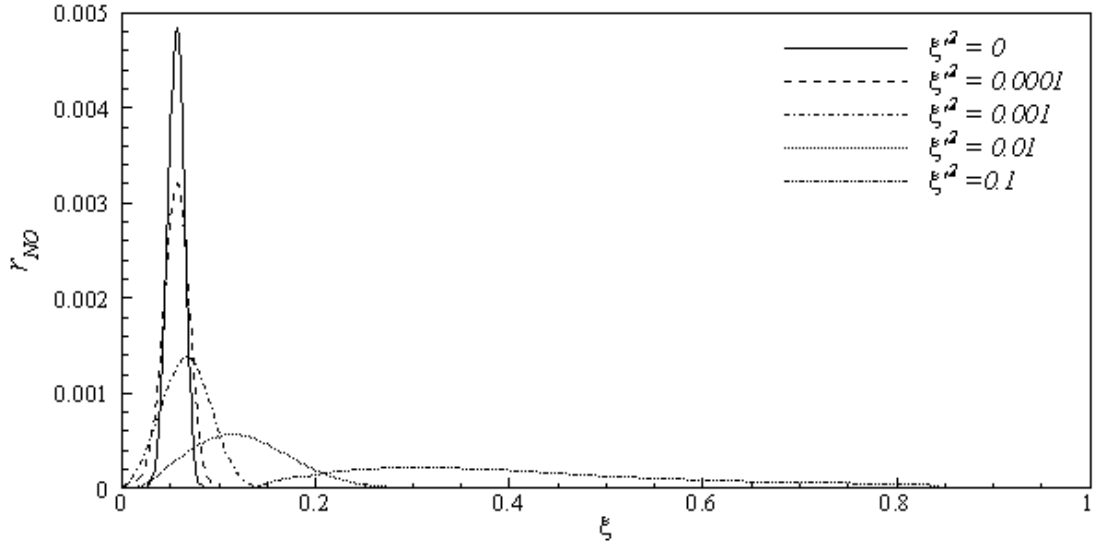

Figure 3. Dependence of the instantaneous *NO* production rate on the mixture fraction and mixture fraction variances

4. Numerical Procedure

For the present simulation, a curvilinear body fitted coordinate system is employed. Inside the combustion chamber the grid consisting of a total of about 1.5 million nodes with a non-uniform mesh distributed along the three co-ordinate directions. As the fuel is injected through a circular nozzle at centre of the combustor inlet at a speed relatively higher than that of the air supplied through the cylinder, a steep gradient appears in this area. To resolve this steep gradient adequately a very fine mesh is required at the centre of the combustor. The mesh lines are contracted at the centre and the inlet of the combustor, and they are expanded smoothly in all the three directions outwards from the centerline and inlet.

The numerical solution procedure is based on the finite volume approach where the governing equations are integrated over the mesh control volume. The finite volume based in-house developed code LES-BOFFIN (Boundary Fitted Flow Integrator) has been used to solve the governing equations. The code is second order accurate in both space and time. The BOFFIN code has been applied extensively in the LES of reacting and non-reacting turbulent flows; for examples, see LES of a turbulent non-premixed propane-ar reacting flame, Paul *et al*. [22], of a gas turbine combustor, di Mare *et al*. [23] and of a turbulent nonpremixed flame, Branley and Jones [24]. Details of the numerical method used in the BOFFIN are not presented here for brevity.

In the simulation fully-developed turbulent pipe flow profiles were applied as the instantaneous inflow boundary conditions at the fuel nozzle, while a uniform velocity profile is applied for the air flow. The mixture fraction at the inlet is defined as

$$\xi = \begin{cases} 1 & \text{in the fuel stream} \\ 0 & \text{in the air stream} \end{cases} \tag{19}$$

The *NO* mass fraction are negligibly small at the inlet and set to zero. Fig. 3 clearly shows that the production rate of *NO* is zero at ξ = 0.0 and 1.0. At the outlet boundary, a non-reflective boundary condition is used, a condition sufficient to minimize the effects of the outlet boundary in the solutions. A thin viscous sub-layer develops adjacent to the walls of the combustor and a prohibitively fine mesh would be required to resolve this. To overcome this difficulty an equilibrium log-law condition is employed as a near wall condition at the surfaces of the combustor.

5. Results and Discussion

We present the computational results in this section. The average time step, *dt*, used in the computation is at the order of 10^{-6}. The results presented here in the form of time mean which are defined as

$$\langle \widetilde{\psi} \rangle = \frac{1}{N} \sum_{n=1}^{N} \widetilde{\psi} \tag{20}$$

where $\widetilde{\psi}$ is the time dependent results of a total of N = 3 x 10^5 time steps.

The results are obtained for two cases, Smagorinsky constant, C_s, of 0.1 (Case 1) and dynamically calibrated C_s (Case 2). The solid lines indicate Case 1 and the dashed lines represent Case 2.

5.1. Temperature and Species Mole Fractions

The results of temperature and species mole fractions, which are required as an input to the *NO* formation model, are presented here.

Computationally predicted mean temperature, $< \widetilde{T} >$, results along axial and radial direction at different cross sectional positions are compared against the experimental measurement done by Nishida and Mukohara [1] in Fig. 4. In Fig. 4(a), at the inlet the predicted mean axial temperature on the centerline is same as the injected fuel temperature. The flame temperature then starts increasing and achieves a maximum value of 1696*K* (Case1) and 1730*K* (Case2) at the outlet. The corresponding peak temperature in the experimental investigation was recorded as 1765*K*, so the computation slightly under predict the temperature at the outlet. But the peak level of the mean temperature is better predicted in Case2. Moreover, the experimental results show a concave like shape around $y = 0.2m$, which is not evident in the predictions where a slight over-prediction is evident in both the cases.

In Fig. 4(b-d), the radial distribution of the mean temperature shows that the peak value of the computed temperature is slightly under-predicted and moves towards the wall near the inlet (frames b, c), and the temperature at the centre shows slight over-prediction in both the Cases. But a slight under-prediction of the temperature occurs at the centre in the downstream (frames d), but a better prediction is found in Case2. Comparing the computed temperature distributions with the experiment, it is found that the trend of increasing and decaying of the temperature in the radial direction is matched reasonably well with the experimental data. However, both quantitatively and qualitatively a very good agreement is achieved with experiment.

In Figs. 5-7, we present the results of the mole fraction of the three selected combustion species and comparisons with those of the experiment are made. Fig. 5(a) shows that the predicted axial mole fraction of the fuel $< \tilde{Y}_{C_3H_8} >$ has an excellent agreement with the experimental result. The mole fraction of the reactant $< \tilde{Y}_{N_2} >$ in Fig. 5(b) is predicted well. While the $< \tilde{Y}_{O_2} >$ in Fig. 5(c) is under-predicted at the downstream but predicted well against the experiment at the upstream. From the radial profiles for reactants $< \tilde{Y}_{C_3H_8} >$, $< \tilde{Y}_{N_2} >$ and $< \tilde{Y}_{O_2} >$ in both locations at y = 0.1m (Fig. 6) and y = 0.3m (Fig. 7), we have a good agreement with the experiment. However, there are slightly over- and under- prediction at some positions but the trend is matched well with experimental measurements.

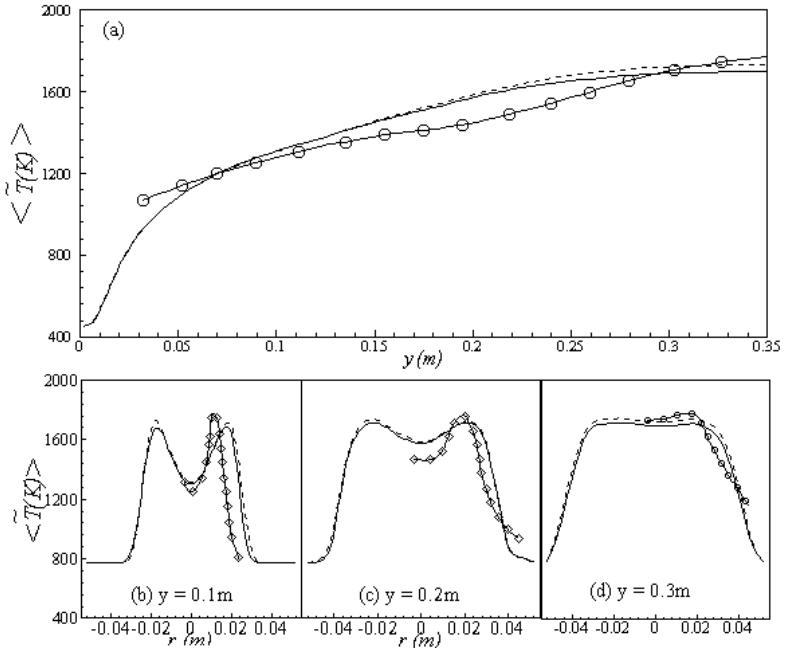

Figure 4. Comparisons of the mean temperature, $<\tilde{T}(K)>$, with those of the experimental data along the (a) axial direction, and the radial direction at different cross-sectional positions: (b) $y = 0.1m$, (c) $y = 0.2m$ and (d) $y = 0.3m$; Solid line, Case1; Dashed line, Case2; Solid line with circle, experimental

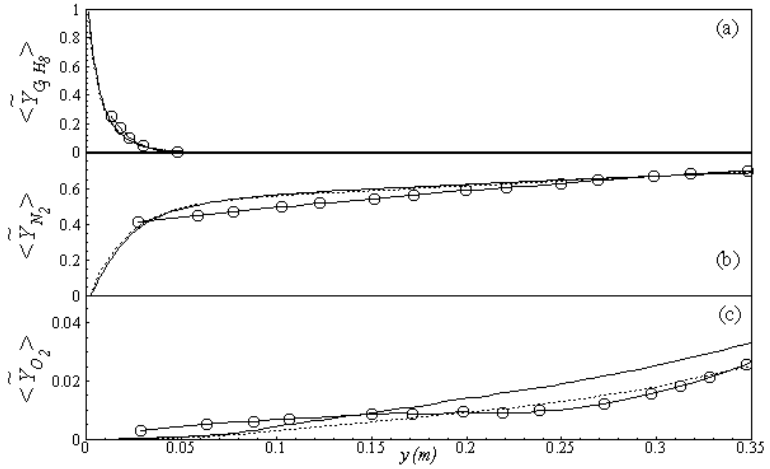

Figure 5. Mean mole fractions: (a) $<\tilde{Y}_{C_3H_8}>$, (b) $<\tilde{Y}_{N_2}>$ and (c) $<\tilde{Y}_{O_2}>$ along the axial direction; Solid line, Case1; Dashed line, Case2; Solid line with circle, experiment

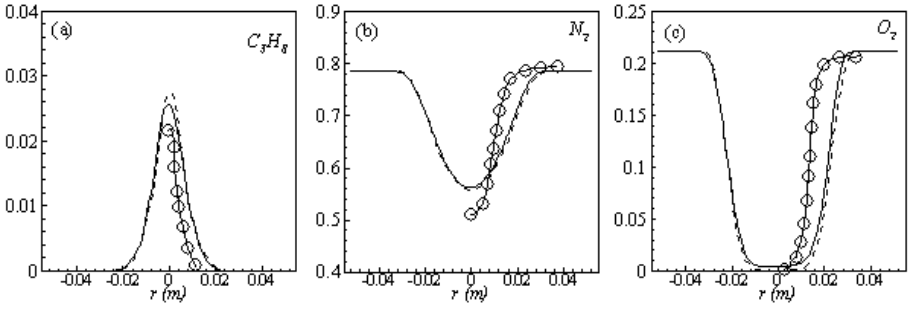

Figure 6. Mean mole fractions: (a) $<\tilde{Y}_{C_3H_8}>$, (b) $<\tilde{Y}_{N_2}>$ and (c) $<\tilde{Y}_{O_2}>$ along the radial direction at $y = 0.1m$; Solid line, Case1; Dashed line, Case2; Solid line with circle, experiment

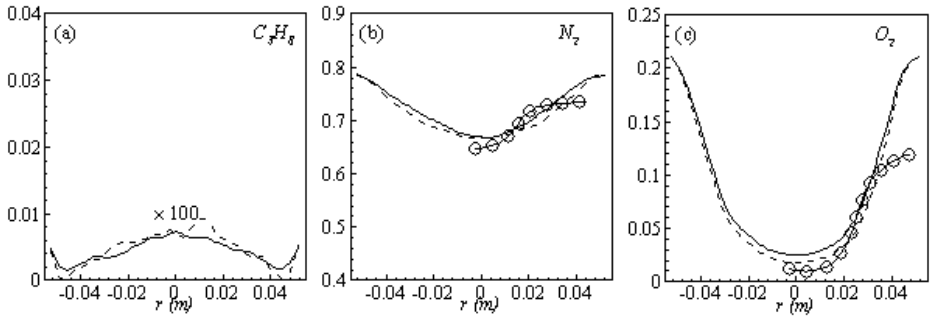

Figure 7. Mean mole fractions: (a) $< \tilde{Y}_{C_3H_8} >$, (b) $< \tilde{Y}_{N_2} >$ and (c) $< \tilde{Y}_{O_2} >$ along the radial direction at $y = 0.3m$; Solid line, Case1; Dashed line, Case2; Solid line with circle, experiment

5.2. Production Rate and Mass Fraction of NO

In Fig. 8 the time averaged results of the (a) temperature, $< \tilde{T}(K) >$, (b) *NO* production rate, $< \tilde{r}_{NO} >$, and (c) mass fraction of *NO*, $< \tilde{Y}_{NO} >$, on the horizontal midplane of the combustor are plotted. The solid lines shown on the contour plots represent the locus of the stoichiometric mixture fraction. These contour plots, obtained in Case1, clearly show that the production of *NO* is highly dependent on both the flame temperature (frame (a)) and the concentration of N_2 (Fig. 5(b)). The mass fraction of *NO* reaches the maximum level at the stoichiometric zone.

Mean axial and radial profiles of the *NO* production rate, $< \tilde{r}_{NO} >$, are depicted in Fig. 9. Axial profile on the centerline of the combustor, plotted in Fig. 9(a), shows that the rate is zero upto the axial distance $y = 0.1$, where the fuel stream dominates, afterwards the rate increases and gets its maximum at the outlet of the combustor. From the radial profile of the *NO* production rate, plotted in Fig. 9(b-d), it can be seen that the peak values are predicted in between the centerline and the combustor wall where the temperature (see Fig. 5(b-d)) as well as the concentration of N_2 (Fig. 6(b), 7(b)) has also its maximum, which can clearly be seen from the mean plot of the *NO* production rate presented in Fig. 8.

Predicted axial profile of the *NO* mass fraction (Fig. 10(a)) increases gradually as the flame temperature increases and achieves a peak level at the outlet of the combustor the maximum temperature (Fig. 4(a)) is recorded. This is simply because the present *NO* formation model includes the Zeldovich or thermal reaction mechanism in which the *NO* production rate is highly dependent on the temperature and reactants (N_2 and O_2). The radial profiles (Figs. 10(b-d)) of the *NO* mass fraction show that the *NO* production level decreases along the radial direction because of the temperature near the combustor wall which is very low although the N_2 level is predicted high in this region.

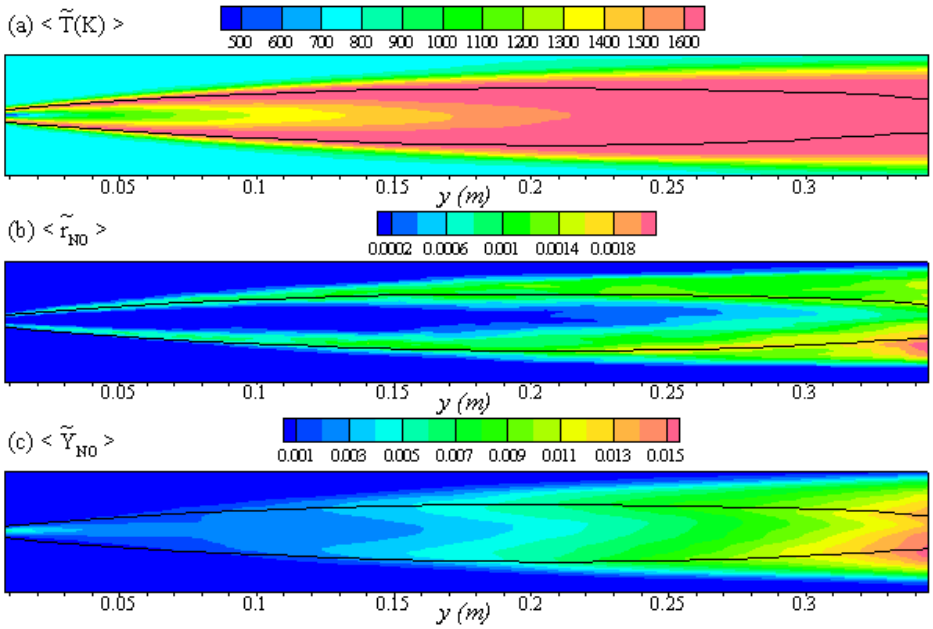

Figure 8. The mean values of the (a) temperature, $< \tilde{T}(K) >$, (b) *NO* production rate, $< \tilde{r}_{NO} >$, and (c) *NO* mass fraction, $< \tilde{Y}_{NO} >$ on the horizontal mid-plane of the combustor, for Case 1

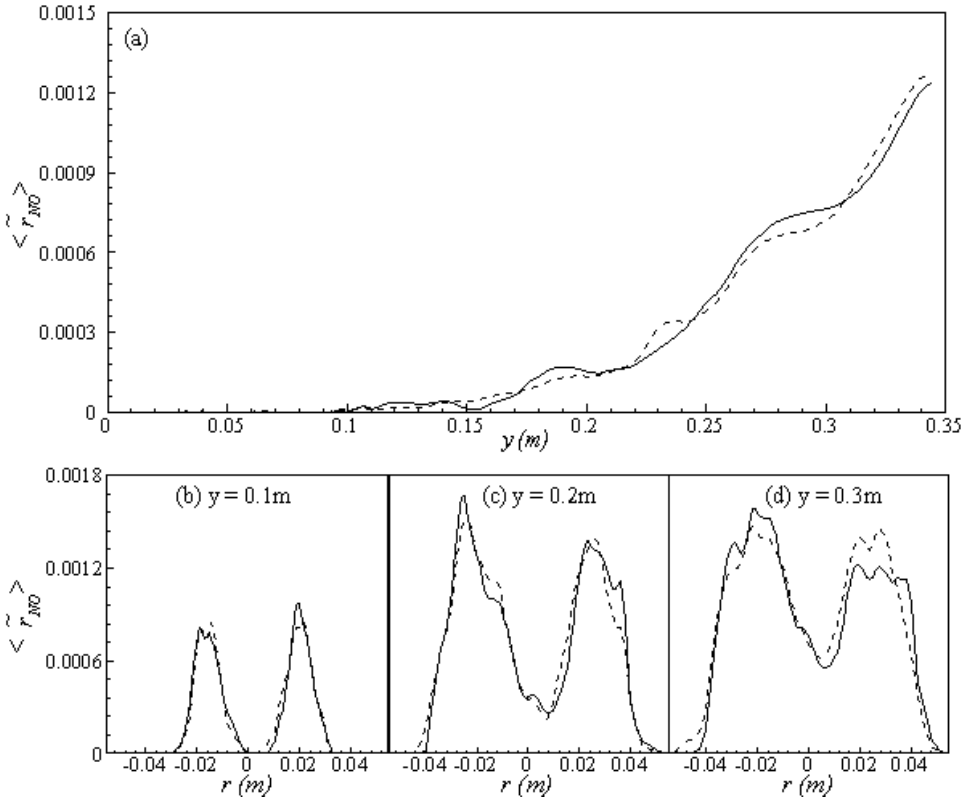

Figure 9. Mean values of *NO* production rate, $< \widetilde{r}_{NO} >$, along the (a) axial direction and radial direction at the different cross-section positions: (b) $y = 0{:}1m$, (c) $y = 0{:}2m$, (d) $y = 0{:}3m$ of the combustor

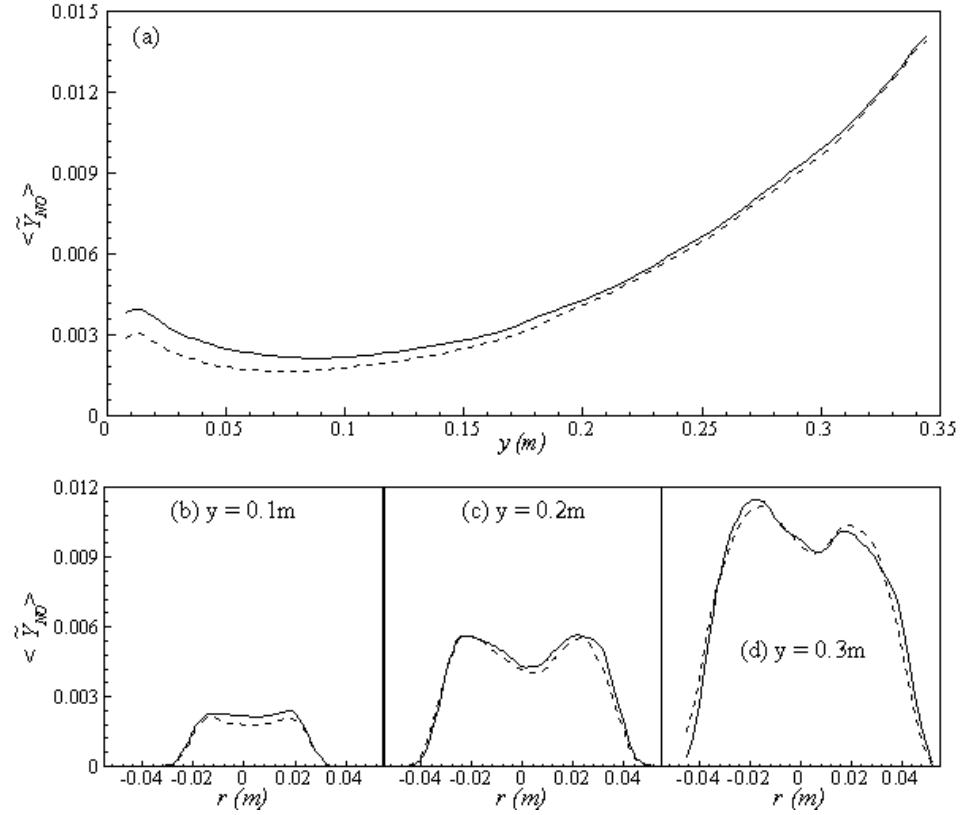

Figure 10. Mean values of the *NO* mass fraction, $< \widetilde{Y}_{NO} >$, along the (a) axial direction and radial direction at the different cross-section positions: (b) $y = 0{:}1m$, (c) $y = 0{:}2m$, (d) $y = 0{:}3m$ of the combustor

Comparison between Case 1 and Case 2 shows that Case 2 produces slightly low levels of the mean *NO* mass fraction in the upstream region, while towards the downstream both predictions gradually converge together.

6. Conclusions

Large Eddy Simulation technique has been applied to investigate the *NO* production in the non-premixed propane/air turbulent combustion process within a cylindrical combustor. In LES a constant valued Smagorinsky model as well as a dynamic model is taken into account for modelling the sub-grid scale stresses. The non-premixed combustion process is modelled through the conserved scalar approach with the laminar flamelet model, while the *NO* production mechanism is modelled through a balance equation for *NO* mass fraction. The extended Zeldovich (thermal) reaction mechanism is taken into account to model the *NO* production.

The computational results of temperature and selected species mole fractions have been compared with the experimental data obtained by Nishida and Mukohara [1] in the turbulent co-flowing propane and preheated air combustion, where a good agreement is achieved.

It was not possible to compare the computational results of the *NO* mass fraction with experimental data, as Nishida and Mukohara [1] did not perform any measurements on the *NO* mass fraction. However, the present results of *NO* clearly agree well with the principle and reaction mechanism of the extended Zeldovich (thermal) used for the modeling of *NO*. The *NO* mass fraction is predicted high in the high temperature zone.

The results are almost uninfluenced by the choice of sub-grid scale models although slightly lower prediction of *NO* mass fraction is found with dynamic *Cs* in the upstream. However, dynamic C_s produces a higher levels of the sub-grid scale quantities in the upstream region.

REFERENCES

[1] O. Nishida, S. Mukohara, Characteristics of Soot Formation and Decomposition in Turbulent Diffusion Flames, *Combustion and Flame* 47 (1982) 269–279.

[2] C. F. Bowman, Control of Combustion-Generated Nitrogen Oxide Emissions: Technology Driven by Regulation, in: *24th Symposium (International) on Combustion*, The Combustion Institute, 1992, pp. 859–878.

[3] J. Zeldovich, The Oxidation of Nitrogen Combustion and Explosions, *Acta Physicochim*. URSS 21 (1946) 577–628.

[4] C. P. Fenimore, Studies of Fuel-Nitrogen Species in Rich Flame Gases, in: *17th Symposium (International) on Combustion*, The combustion institute, Philadelphia, PA, 1979, pp. 661–669.

[5] P. Meunier, M. Costa, M. G. Carvalho, On NO_x Emissions from Turbulent Propane Diffusion Flames, *Combustion and Flame* 112 (1998) 221–230.

[6] H. S. Kim, S. W. Baek, M. J. Yu, Formation Characteristics of Nitric Oxide in a Three-Stages Air/LPG Flame, *International Journal of Heat and Mass Transfer* 46 (2003) 2993–3008.

[7] N. Taniguchi, T. Tominaga, K. Inoue, M. Hirohata, T. Kobayashi, A Large Eddy Simulation of Non-premixed Turbulent Flame and Nitric Oxide Production, in: *4th International Symposium on Turbulence, Heat and Mass Transfer*, Begell House, Inc., 2003, pp. 1–6.

[8] M. Ihme and H. Pitsch, Modeling of radiation and nitric oxide formation in turbulent nonpremixed flames using a flamelet/progress variable formulation. *Physics of Fluids* 20 (2008) 055110.

[9] K. W. Chun, H. J. Chung, S. H. Chung, J. H. Choi, A numerical study on extinction and NOx formation in nonpremixed flames with syngas fuel. *Journal of Mechanical Science and Technology* 25 (11) (2011) 2943-2949.

[10] D. L. Baulch, C. J. Cobos, R. R. Cox, *et al*, Evaluated Kinetic Data for Combustion Modeling, *Journal of Physical and Chemical Reference Data* 21 (3) (1992) 411–734.

[11] D. L. Baulch, C. J. Cobos, R. R. Cox, *et al*, Summary Table of Evaluated Kinetic Data for Combustion Modeling: Supplement-1, *Combustion and Flame* 98 (1994) 59–79.

[12] A. Leonard, Energy Cascade in Large-Eddy Simulations of Turbulent Fluid Flows, *Advances in Geophysics* 18(A) (1974) 237–248. [11] A. Favre, Statistical Equations of Turbulent Cases in Problems of Hydrodynamics and Continuum Mechanics, Tech. rep., Society of Industrial and Applied Mathematics, Philadelphia (1969).

[13] A. Favre, Stastical equations of turbulent gases. In: Problems of hydrodynamicsand continuum mechanics, Technical report, Society of Industrial and Applied Mathematics, Philadelphia; 1969.

[14] K. M. Leung, Kinetic modelling of hydrocarbon ames using detailed and systemically reduced chemistry, PhD thesis, Department of Chemical Engineering, Imperical College London (1996).

[15] M. Fairweather, W. P. Jones, H. S. Ledin, R. P. Lindstedt, Predictions of Soot Formation in Turbulent, Non-Premixed Propane Flames, in: *24th Symposium* (*International*) *on Combustion*, The Combustion Institute, 1992, pp. 1067–1074.

[16] S. C. Paul, Large Eddy Simulation of a Fuel-Rich Turbulent Non- Premixed Reacting Flow With Radiative Heat Transfer, Department of Mechanical Engineering, University of Glasgow, (2008) PhD thesis.

[17] J. Smagorinsky, General Circulation Experiments with the Primitive Equations-I. The Basic Experiment, *Monthly Weather Review* 91(3) (1963) 99–164.

[18] M. Germano, U. Piomelli, P. Moin, W. H. Cabot, A Dynamic Subgrid-Scale Eddy Viscosity Model, *Physics of Fluids A* 3(7) (1991) 1760–1765.

[19] H. Schmidt, U. Schumann, Coherent Structure of the Convective Boundary Layer Derived from Large-Eddy Simulations, *Journal of Fluid Mechanics* 200 (1989)

511–562.

[20] N. Peters, Laminar Diffusion Flamelet Models in Non-Premixed Turbulent Combustion, *Progress in Energy and Combustion Science* 10 (1984) 319–339.

[21] R. W. Bilger, Turbulent flows with nonpremixed reactants, in: P. A. Libby, F. A. Williams (Eds.), *Turbulent Reactings Flows*, Springer-Verleg, Heidelburg, 1980, Ch. 3, pp. 65–113.

[22] S. C. Paul, M. C. Paul, W. P. Jones, Large Eddy Simulation of a turbulent non-premixed propane-air reacting flame in a cylindrical combustor, *Computer & Fluids*, 39(2010) 1832-1847.

[23] F. di Mare, W. P. Jones, K. R. Menzies, Large Eddy Simulation of a Model Gas Turbine Combustor, *Combustion and Flame* 137 (2004) 278–294.

[24] N. Branley, W. P. Jones, Large Eddy Simulation of a Turbulent Nonpremixed Flame, *Combustion and Flame* 127 (2001) 1914–1934.